Supporting Information for "Direct Simulation of the Self-Assembly of a Small DNA Origami"

Benedict E. K. Snodin,* Flavio Romano, Lorenzo Rovigatti, Thomas E. Ouldridge, Ard A. Louis, and Jonathan P. K. Doye*

E-mail: benedict.snodin@chem.ox.ac.uk; jonathan.doye@chem.ox.ac.uk

Table S1: The simulation parameters used in the input file for the oxDNA code when running the simulations used to obtain the results described in this work.

Parameter	Value
newtonian_steps	103
diff_coef	2.5
thermostat	brownian
dt	0.005
verlet_skin	0.05

Time scale estimation. To convert our simulation time units to physical units, we consider the on-rate for a 16-base-pair duplex section. For the experimental figure, we use an approximate rate constant suggested by experimental measurements[1–7] for a 16-base-pair duplex of $10^6\,\mathrm{M}^{-1}\,\mathrm{s}^{-1}$. We then compare this to a similar transition computed using oxDNA, namely the binding of the first scaffold domain (16 base pairs long) in the self-assembly of an origami design (design B) similar to the design used for this work (design A).[1] Clearly, the simulated system (one stage of an origami assembly) is somewhat different to the experimental one (formation of a simple 16-base-pair duplex), but we believe that this difference is not too important for this very rough time scale estimation.

[1]Like design A, all of design B's scaffold domains are 16 base pairs in length, and in both cases there are 24 such scaffold domains. However, each of design B's staples are 48 bases long and bind to three scaffold domains, unlike design A's staples which are 32 bases long and only bind to two scaffold domains.

The simulated on-rate (computed using forward-flux sampling) is 1.0×10^{-10} per simulation time unit, measured at a concentration of 1.0×10^{-8} M. The experimentally determined on-rate at this concentration is $10^{6}\,\mathrm{M}^{-1}\,\mathrm{s}^{-1} \times 10^{-8}\,\mathrm{M} = 10^{-2}\,\mathrm{s}^{-1}$. Thus, the unit conversion is given by

$$\frac{1.0 \times 10^{-10} \text{ per simulation time unit}}{10^{-2}\,\mathrm{s}^{-1}} \approx 10^{-8}\,\mathrm{s} \text{ per simulation time unit} \qquad (1)$$

Table S2: DNA strand sequences used for the assembly simulations described in this paper. Sequences were obtained with NUPACK with a search designed to minimize secondary structure and intra-staple binding. The "Scaffold Domain" column indicates which scaffold domains the staple strands bind to (see Fig. 1.

Strand	Scaffold Domains	Sequence
scaffold	-	ATGCAAAGATACGGAAAAGGGAGAGAAAGAAG
		AGGGACACGGGAAAGGGCAAAAAAACAAAGAA
		TGGGAGTAGGAAGCGAGAAAATAACGGGCAGC
		TATAAAGAAAAAAAGGGAAAGATAGAACAGGG
		AGGAGGAAAGAGACAGTAGAGTGGTGATAGGG
		AGAAGAAAAGAAGAAAAAGAGGAGAGCAAGAA
		ACGGGATAGAGAAGAGGAACAGCAAAAGACAA
		AGAAGAGGGGCAAGAGAGGATAGAAGTACGAG
		ATAAGGGGTAGAAGCGAAAAGCAAAAAATAAG
		GGATAAGAGACGGGGAGAAGTGAAGAAAGAAG
		GAGGATAAAAAGACAGATGGACACGAAAGGAA
		GATAGGAGGGGGAGCGACGAATAAAAGGAAAC
staple 1	1, 2	CTTCTTTCTCTCCCTTTTCCGTATCTTTGCAT
staple 2	3, 4	CCTTTCCCGTGTCCCTTTCTTTGTTTTTTTGC
staple 3	5, 8	CCCTGTTCTATCTTTCTCGCTTCCTACTCCCA
staple 4	6, 7	GCTGCCCGTTATTTTCCCTTTTTTTCTTTATA
staple 5	9, 10	CTGTCTCTTTCCTCCTCCCTATCACCACTCTA
staple 6	11, 14	TTGTCTTTTGCTGTTCTTTCTTCTTTTCTTCT
staple 7	12, 13	TTCTTGCTCTCCTCTTCTCTTCTCTATCCCGT
staple 8	15, 16	CTCTTGCCCCTCTTCTCTCGTACTTCTATCCT
staple 9	17, 20	CTTCTTTCTTCACTTCCGCTTCTACCCCTTAT
staple 10	18, 19	CTTATTTTTTGCTTTTTCCCCGTCTCTTATCC
staple 11	21, 22	CTGTCTTTTTATCCTCTTCCTTTCGTGTCCAT
staple 12	23, 24	GTTTCCTTTTATTCGTCGCTCCCCCTCCTATC

Additional simulations and simulation snapshots. Fig. S1 shows typical configurations at the beginning of an excess-staple assembly simulation and a stoichiometric assembly

simulation, Fig. S1(a) illustrating the high concentration used for the excess-staple assembly simulations. Fig. S2 shows the kymographs for the three further excess-staple simulations at 65 °C. They show similar behaviour to Fig. 2, but in these instances assembly has not progressed as far. Fig. S3 shows the kymographs for stoichiometric assembly simulations at 55 °C and 70 °C. They show a pattern of behaviour with temperature consistent with that seen in the kymographs shown in Fig. 8. At 55 °C there is a degree of misbonding that is intermediate between that shown in Fig. 2 for 50 °C and 60 °C, and at 70 °C the progress of assembly is even slower than at 65 °C due to the reduced rate of domain binding.

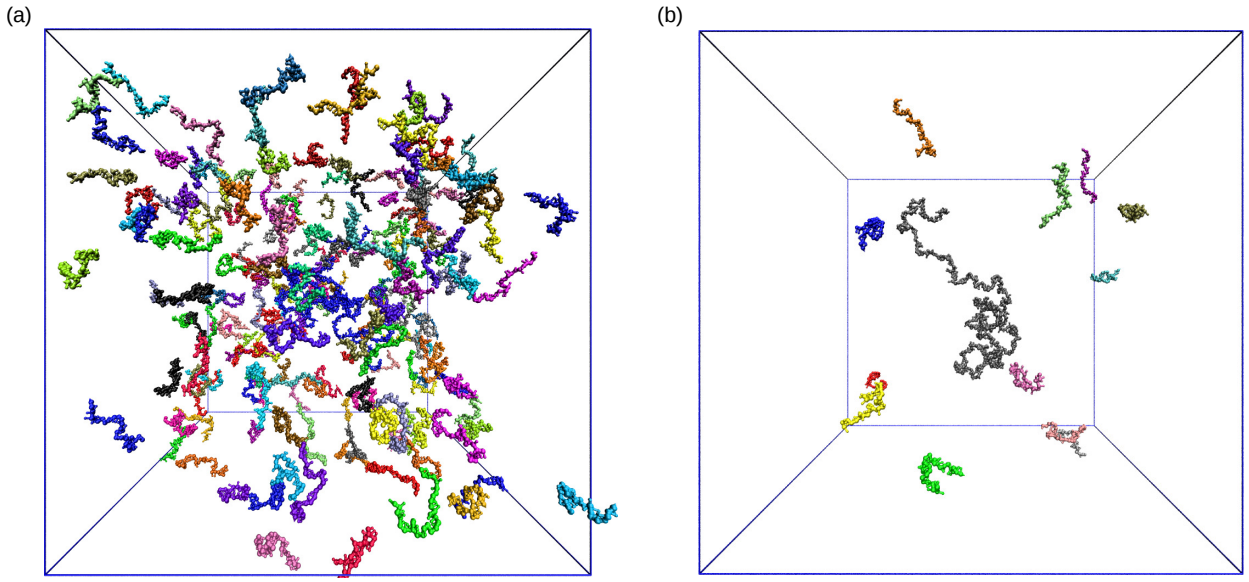

Figure S1: Snapshots from the beginning of an assembly simulation for (a) the excess-staple assembly and (b) the stoichiometric assembly. The box shows the location of the periodic boundaries.

Geometric descriptors for the complete assembly. For the trajectory illustrated in Fig. 8(b) and Fig. 9, in which a complete origami formed, we show how various geometric descriptors of the assembly change with time in Fig. S4.

The shortest distance between each staple and its complementary scaffold domains, averaged over all staples, is plotted in Fig. S4(a), while the average distance between each staple's centre of mass and that of its closest neighbouring staple is plotted in Fig. S4(c). Both of these show significant fluctuations as the strands diffuse around the box, with the

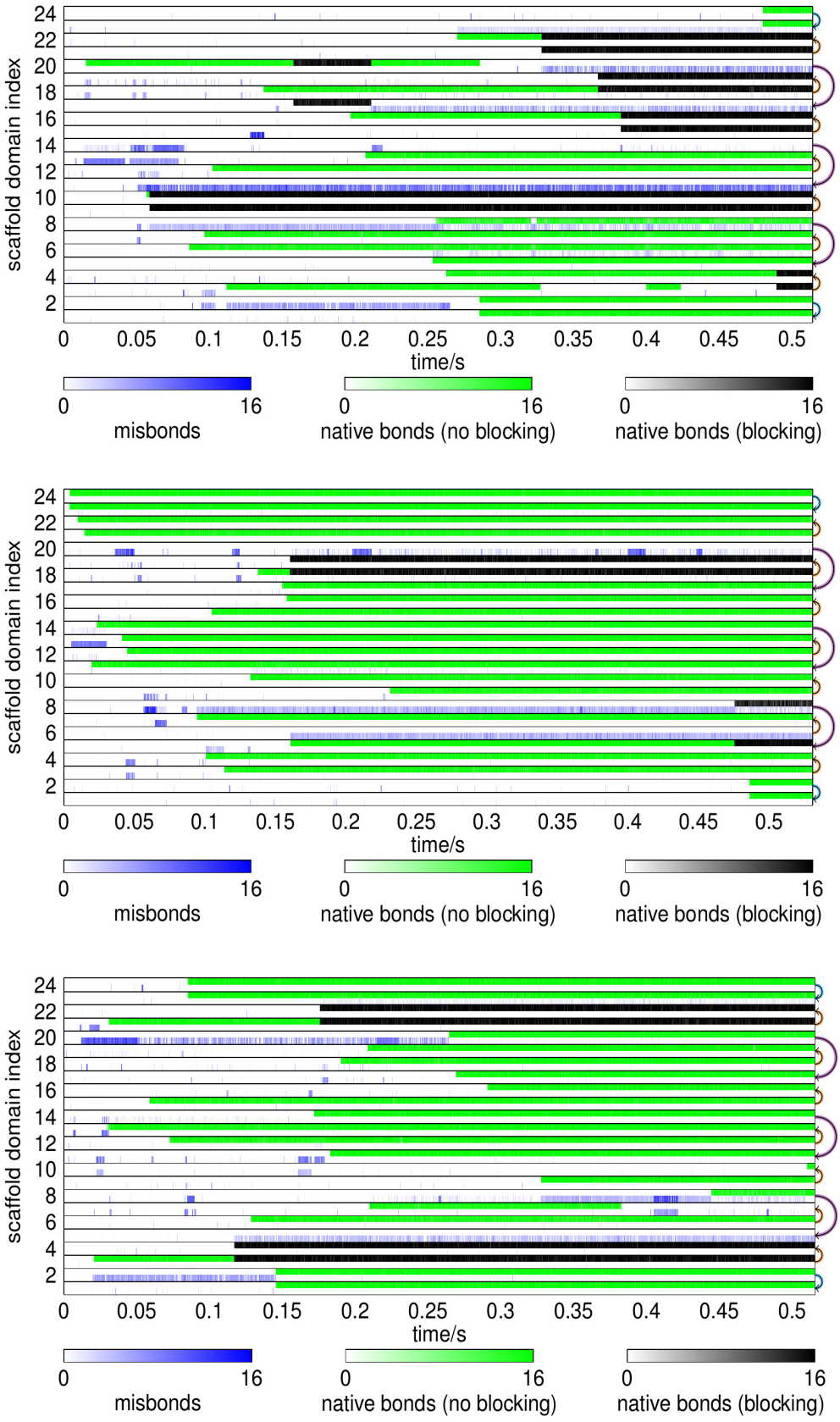

Figure S2: Kymographs for the three further simulations at 65 °C with a 17× excess of staples.

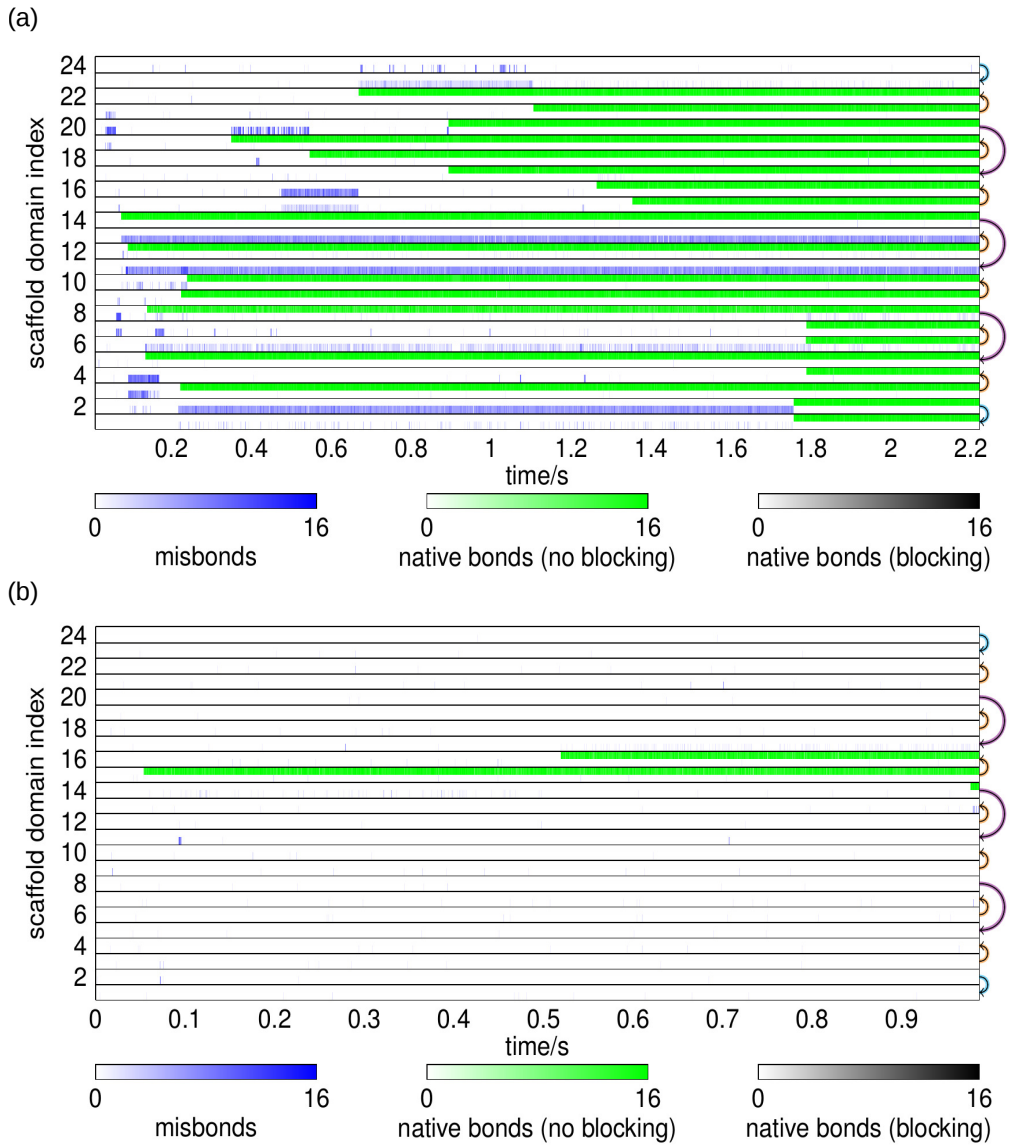

Figure S3: Kymographs for stoichiometric assembly simulations at (a) 55 °C and (b) 70 °C.

fluctuations and mean values decreasing after staple binding events. To illustrate the behaviour of a single staple, Fig. S4(b) shows the shortest distance between scaffold domains 23 and 24 and the staple that binds to those domains. The distance fluctuates greatly as the staple strand and scaffold strand diffuse through the box, often passing very close to each other, until finally the staple binds to the scaffold and the distance and fluctuations become very small.

Fig. S4(d) shows how the structure of the scaffold strand, as measured by its radius of gyration, evolves with time. It can be clearly seen that the scaffold becomes more compact as the assembly of the origami progresses. Furthermore, the fluctuations in the radius of gyration also decrease as assembly progresses. However, even when assembled there are still substantial fluctuations in the shape of the origami. Although signficant shape fluctuations are likely to occur for any two-dimensional origami in solution, these fluctuations are particularly large for our small origami, because of the relatively small number of constraining junctions.

Comparing Figs. S4(a), (c) and (d), it is noticeable that, whereas the average distance plots show a relatively steady decrease as the number of bound staples increases, the radius of gyration does not change much when the first staples bind, but only starts to decrease significantly between 1.2 and 1.5 s (see Fig. 8(b)), a period in which eight staple domains bind and key junctions form that significantly constrain the structure of the scaffold.

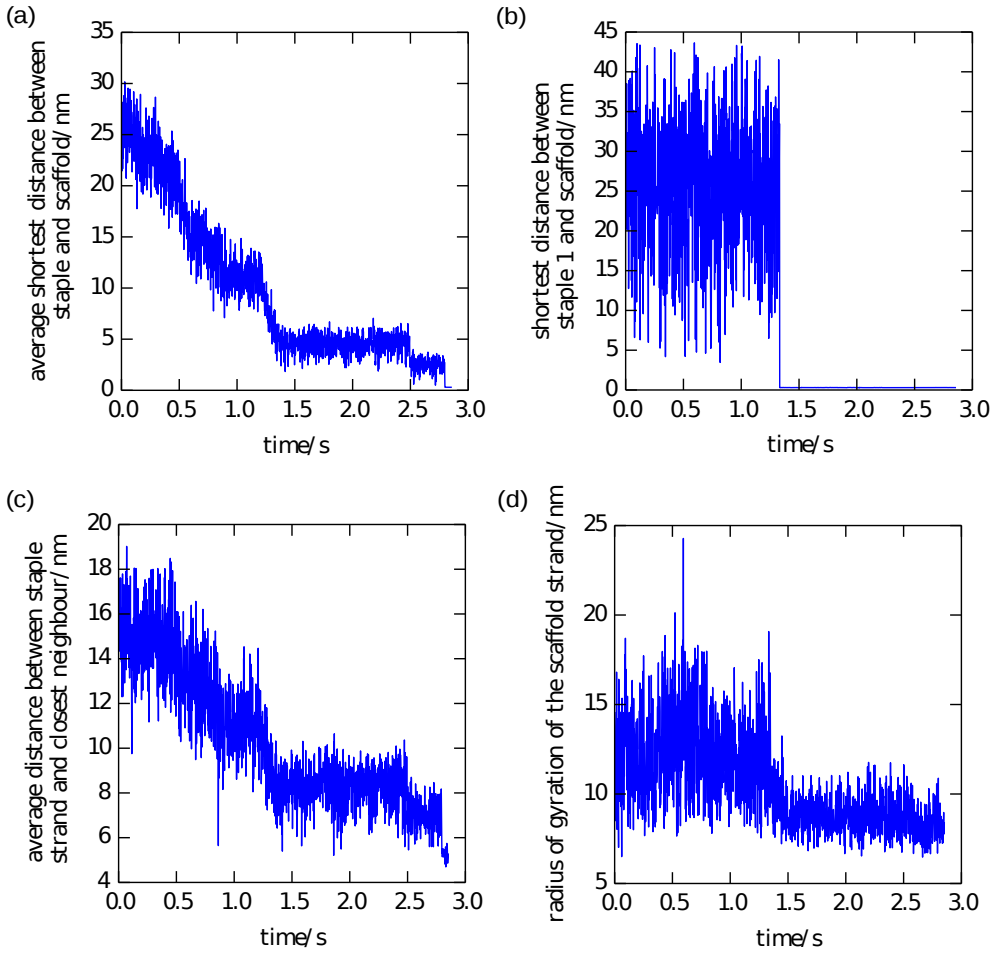

Figure S4: Various geometric descriptors as a function of time for the stoichiometric assembly simulation at 60 °C illustrated in Fig. 8(b) and 9 in which a complete origami successfully formed. (a) The shortest distance between each staple and its complementary scaffold domains, averaged over all staples. This decreases during the simulation as more staples bind to the scaffold. (b) The shortest distance between staple 1 and the scaffold domains to which it binds, namely domains 23 and 24. This distance fluctuates greatly as the staple and scaffold diffuse around the simulation box, until the staple binds to the scaffold and the distance is reduced almost to zero. (c) The average distance between DNA strand centre of masses for each staple and its closest neighbour. This decreases during the simulation due to staples binding to the scaffold, similarly to (a). (d) The radius of gyration of the scaffold strand. The radius of gyration decreases with time as the assembly progresses and the scaffold strand becomes more constrained by staple crossovers.

References

1. Gao, Y.; Wolf, L. K.; Georgiadis, R. M. Secondary Structure Effects on DNA Hybridization Kinetics: a Solution *versus* Surface Comparison. *Nucleic Acids Res.* **2006**, *34*, 3370–3377.

2. Morrison, L. E.; Stols, L. M. Sensitive Fluorescence-Based Thermodynamic and Kinetic Measurements of DNA Hybridization in Solution. *Biochemistry* **1993**, *32*, 3095–3104.

3. Zhang, D. Y.; Winfree, E. Control of DNA Strand Displacement Kinetics Using Toehold Exchange. *J. Am. Chem. Soc.* **2009**, *131*, 17303–17314.

4. Craig, E. M.; Crothers, M. D.; Doty, P. Relaxation Kinetics of Dimer Formation by Self Complementary Oligonucleotides. *J. Mol. Biol.* **1971**, *62*, 383–392.

5. Pörschke, D.; Eigen, M. Co-Operative Non-Enzymatic Base Recognition III. Kinetics of the Helix-Coil Transition of the Oligoribouridylic - Oligoriboadenylic Acid System and of Oligoriboadenylic Acid Alone at Acidic pH. *J. Mol. Biol.* **1971**, *62*, 361–364.

6. Pörschke, D.; Uhlenbeck, O. C.; Martin, F. H. Thermodynamics and Kinetics of the Helix-Coil Transition of Oligomers Containing GC Base Pairs. *Biopolymers* **1973**, *12*, 1313–1335.

7. Chen, C.; Wang, W.; Wang, Z.; Wei, F.; Zhao, X. S. Influence of Secondary Structure on Kinetics and Reaction Mechanism of DNA Hybridization. *Nucleic Acids Res.* **2007**, *35*, 2875–2884.